Published in final edited form as:

Phys Rev X. 2018 ; 8(4): . doi:10.1103/PhysRevX.8.041014.

Rapid evolution of the Photosystem II electronic structure during water splitting

Katherine M. Davis[1,†], **Brendan T. Sullivan**[1,‡], **Mark C. Palenik**[§], **Lifen Yan**[1], **Vatsal Purohit**[1,¥], **Gregory Robison**[1,¶], **Irina Kosheleva**[2], **Robert W. Henning**[2], **Gerald T. Seidler**[3], and **Yulia Pushkar**[1,*]

[1]Department of Physics and Astronomy, Purdue University, West Lafayette, IN 47907, USA.

[2]Center for Advanced Radiation Sources, The University of Chicago, Chicago, IL 60637, USA.

[3]Department of Physics, University of Washington, Seattle, WA 98195, USA.

Abstract

Photosynthetic water oxidation is a fundamental process that sustains the biosphere. A Mn_4Ca cluster embedded in the photosystem II protein environment is responsible for the production of atmospheric oxygen. Here, time-resolved x-ray emission spectroscopy (XES) was used to observe the process of oxygen formation in real time. These experiments reveal that the oxygen evolution step, initiated by three sequential laser flashes, is accompanied by rapid (within 50 μs) changes to the Mn Kβ XES spectrum. However, no oxidation of the Mn_4Ca core above the all MnIV state was detected to precede O−O bond formation, and the observed changes were therefore assigned to O−O bond formation dynamics. We propose that O−O bond formation occurs prior to the transfer of the final (4th) electron from the Mn_4Ca cluster to the oxidized tyrosine Y_Z residue. This model resolves the kinetic limitations associated with O−O bond formation, and suggests an evolutionary adaptation to avoid releasing of harmful peroxide species.

Enzymes function as nature’s catalysts, facilitating virtually all the reactions necessary for life. By carefully coordinating electron dynamics and atomic rearrangements within a predefined energy landscape, they enable a broad range of efficient and highly selective transformations, many of which have proven challenging for chemists. Among these, the reaction catalyzed by the Mn_4Ca cluster of photosystem II (PS II) during photosynthesis holds a special place, as the ability to biosynthesize O_2 from H_2O occurred only once during evolution 3. The development of this process dramatically altered our planet by generating the oxygen-rich atmosphere we live in today. The catalytic activity and quantum efficiency of the oxygen evolving complex (OEC) remain unmatched by synthetic systems developed

*Correspondence to: ypushkar@purdue.edu.
†Department of Chemistry, Princeton University, Princeton, NJ 08544, USA.
‡Neutron Scattering Division, Oak Ridge National Laboratory, Oak Ridge, TN 37830, USA.
§Naval research laboratory, Washington, DC 20375, USA.
¥Department of Biology, Purdue University, West Lafayette, IN 47907, USA.
¶Department of Physics and Astronomy, Hanover College, Hanover, IN 47243, USA.

Supporting Information. Materials and methods, Figures S1–S4, and Tables S1 & S2.

for artificial photosynthesis `. Despite its far-reaching consequences, the underlying mechanism of PS II remains debated.

In 1970, Bessel Kok *et al.* described a potential water splitting mechanism in which the OEC cycles through five states (S_0-S_4), corresponding to the oxidation states of manganese, following sequential visible light absorptions, Figure 1A [1]. Antenna pigments from the surrounding protein matrix absorb these photons and funnel energy towards P_{680}, the chlorophyll *a* special pair responsible for charge separation. Within nanoseconds, the tyrosine Y_Z residue (Tyr_Z) located between P_{680} and the OEC is oxidized by the special pair. Tyr_Z• is subsequently reduced by the OEC on a microsecond timescale. This process drives the water splitting reaction [2].

The past forty years have yielded new insights into the structure of PS II [3–12], as well as the nature and timing of the S-state transitions that form the Kok cycle, Figure 1A [13–17]. Nonetheless, the critical step during which the O−O bond is formed remains poorly characterized and thus cannot be implemented in artificial systems. O−O bond formation likely occurs on a microsecond timescale during the S_3 to S_0 transient step of the catalytic cycle, culminating in O_2 evolution. Direct monitoring of this transient process however, has proven challenging and details remain elusive. A pre-eminent report by Babcock et al., as well as recent studies by Nilsson *et al.*, support a rate of Tyr_Z• reduction with $t_{1/2}$ ~1 ms following three flashes, and associate this rate constant with the formation of the S_4-state, subsequently capable of fast O_2 evolution [18,19]. It was pointed out later that such hypotheses face a serious kinetic challenge in that the timescale of molecular oxygen release, following the formation of the S_4-state, is very short for the associated redox chemistry and bond formation dynamics [20]. As an alternative hypothesis, S_3-state peroxide formation was proposed [20], but this has not yet been confirmed experimentally.

Given the lack of definitive spectroscopic results, computational simulations have been performed to model the O−O bond formation path [21–24]. Many of these imply oxidation of the OEC past Mn_4IV via the formation of a MnVMn_3IV state, also presented as Mn_4IV −O• (oxyl radical). This oxidized configuration is currently associated with S_4 and would precede O−O bond formation [21,25]. Experimental proof for a MnVMn_3IV intermediate state is currently lacking, and our data rule out its formation. Here, we examine the earliest dynamic in the S_3 to S_0 transition via time-resolved x-ray emission spectroscopy (TR-XES) utilizing dispersive detection to aid our understanding of this critical biological process [26,27]. In 2015, we proposed a new mechanistic model in which O−O bond formation occurs prior to transfer of the final (4th) electron from the Mn_4Ca cluster to explain our preliminary spectroscopic results [28]. An x-ray crystallographic study of the S_3-state [10] recently confirmed our DFT-based proposal, producing a virtually indistinguishable S_3-state model, within the experimental resolution of x-ray diffraction [29].

Here, we deliver an extensive statistical analysis of these initial datasets in conjunction with those collected subsequently, each consistently composed of almost a half million repetitive interrogations of the OEC electronic structure. The power of large statistical data sets has long been realized in science, often enabling the development of new research tools. A single, blurry electron microscopy image of a complex biomolecule, for instance, provides

little insight into its structure, while several thousand images can now deliver atomically-resolved models [30]. In a similar fashion, repetitive measurement of a spectroscopic response has allowed us to solidify the rapid electronic structure evolution in the S_3 to S_0 transition, a result which is required to complete the description of O−O bond formation in natural photosynthesis.

Mn Kβ spectral emission lines reflect the number of unpaired $3d$ electrons and, thus, provide information about the oxidation and/or spin states for a given Mn ion, inaccessible via structural methods such as x-ray crystallography [31]. The exchange interaction between the $3p$ hole and $3d$ valence electrons in the final state causes multiplet splitting that results in separate $K\beta_{1,3}$ and $K\beta'$ peaks, Figure 1B, C. This coupling is directly linked to the electronic state of Mn such that an increase in the oxidation state results in decreased splitting between the Kβ spectral lines. This effect is most apparent in the $K\beta_{1,3}$ peak position shift to lower energies with increasing oxidation. XES also allows for dispersive detection, in which the full emission spectrum is recorded during a single, intense, polychromatic x-ray pulse, Figure 1D [26]. The temporal resolution of such a setup is limited in practice only by the time structure of the x-ray source. In our experiments, we utilized multi-bunch x-ray exposures of 22 μs to 44 μs duration to match the microsecond kinetics of the OEC [13], Table 1 & Figure S1A. We previously determined exposures of up to 66 μs under these conditions to be undamaging to PS II [26,32]. Data collection was performed using a von Hamos style miniature x-ray emission spectrometer (miniXES – Figure S1B) [26,33], and a non-jet open-air sample delivery system (see SI and Figure S1C) was used to supply fresh, unrecycled PS II for each measurement at a controlled repetition rate. Samples were excited given a defined number (0–3) of laser flashes (F) and probed at a time (Δt) after the final laser flash by a single x-ray pulse, Figures 1D & S1A, Table S1. For clarity, we note that 0F, corresponding to no flashes, corresponds to majority state S_1, 1F corresponds to majority state S_2, etc.

A total of seven beamtimes were accomplished, with two devoted to methodology development and five to data collection (note that dataset #5 was recorded after a beamline upgrade and is analyzed separately), ultimately accumulating over two million x-ray pulses to measure different S-states, Table 2. Time-resolved spectra of the majority S-states S_1, S_2, and S_3 were collected following zero, one and two laser flashes with spacing between consecutive laser flashes of 100 ms, corresponding to a laser frequency of 10 Hz. Samples were probed with the x-ray beam following a Δt=500 μs time delay from the final laser flash to allow for the full reduction of $Tyr_Z^{\bullet}$ with limited decay of the formed S-state, Table S1 [13,34]. Given the multiplet character of the spectra and the noise inherent for such a dilute biological sample, previous studies recommend the use of the statistical first moment, $\frac{\sum_j E_j I_j}{\sum_j I_j}$, surrounding the $K\beta_{1,3}$ peak, to determine any changes to the electronic structure, Figures 2 & 3 [35]. It has been reported, and should be emphasized here, that any data manipulation such as background subtraction and smoothing can affect first moment magnitudes, leading to risk of misinterpretation of small spectral changes [17]. To avoid uncertainties due to these processing methods, we provide the first ever analysis of primary photosystem II emission data. These data sets were subject to no manipulation beyond

extraction of spectra via energy calibration of the detector. The statistical significance of the observed spectral changes is then determined using one-way ANOVA (ANalysis Of VAriance), a simple statistical method employed broadly across many scientific disciplines. Resultant *p*-values represent the probability of falsely rejecting the null hypothesis, i.e. that a difference in the first moment between the two states listed is a random statistical variation. Thus, the lower the *p*-value, the stronger the evidence for changes in the spectra between compared data sets. In this study we take the 95% confidence interval to be significant. Here, background subtraction and smoothing is only used to produce figures for comparison with previous XES PS II studies, which all present significantly processed data.

While it is common to analyze first moments calculated over 6485–6495 eV, this approach fails to convey the full information content of XES spectra. To show that our trends are not dependent on a particular range chosen for analysis of the 1st moment, *p*-contours over variable energy integration ranges are shown in Figures 2, 3, & S3. It is evident that merged data are dominated by statistically significant shifts, with the exception of 1F to 2F, in agreement with earlier work [35]. Note that corners of the contour maps, which either encompass integration ranges outside the peak position, or incomplete portions of the peak, may be influenced more significantly by noise. This is especially true for contours maps of individual beamtimes.

S_1 to S_2-state transition.

The obtained S_1 state spectral shape and peak position are in good agreement with previous RT PS II measurements [26]. A comparison of 0F and 1F first moments evaluated by one-way ANOVA shows a reproducible, statistically significant shift of the $K\beta_{1,3}$ peak to lower energies, Table 3 & Figures 2 & S4. Cryogenic measurements previously reported a −0.059 eV shift following spectral smoothing and background subtraction procedures [35]. Analysis of three combined data sets (#1, 2, and 3) following similar data processing yields a first moment shift of −0.16 eV for our 0F → 1F transition (note that dataset #4 was measured without the S_2-state, and #5 was measured after beamline update is analyzed separately). The observed shift of the $K\beta_{1,3}$ peak to lower energies following a single laser flash is likewise consistent with previous cryogenic XANES [8,36] and recently published room-temperature XES [17] results for the S_1 to S_2 state transition, both of which indicate Mn-centered oxidation. X-ray free electron laser (xFEL)-based TR-XES experiments have struggled to reproduce this result, likely due to a combination of lower spectrometer resolution and data processing methods [27]. Although some xFEL studies [37,38] have observed spectral shifts for x-ray measurements made following a different number of laser flashes, they have not yet provided any new mechanistic insights. Overall, we consider our results for the 0F → 1F transition robust and in good agreement with previous characterization of the S_1 to S_2 transition in which one Mn center is oxidized from MnIII to MnIV.

S_2 to S_3 state transition.

For the ensuing S-state transition, $S_2 \rightarrow S_3$, previous cryogenic measurements determined that changes to the Mn Kβ emission spectrum are minimal, and a small (−0.02 eV) shift, on

the order of our systematic error (0.02 eV, see SI for more details), was reported [35]. A comparison of our 1F and 2F first moments, analyzed with one-way ANOVA indicates a lack of statistical significance over most energy ranges, Table 3 & Figures 2 & S4. Any associated spectral differences are likely too small to reach statistical significance under our experimental conditions. In contrast to both these measurements and earlier XAS studies [8,32,33], Zaharieva et al. recently observed a shift in the room temperature emission spectrum equivalent to that observed during the $S_1 \rightarrow S_2$ transition [17]. Although the proposed Mn oxidation to form Mn_4IV in the S_3 state [39–43] Figure 1A, at its most basic, suggests a comparable XES shift for $S_1 \rightarrow S_2$ and $S_2 \rightarrow S_3$ transitions, we now know that the OEC undergoes a major structural change during the $S_2 \rightarrow S_3$ transition from both extended x-ray fine structure (EXAFS) [36], femtosecond (fs) x-ray crystallography [9–11], and electron paramagnetic resonance (EPR) [42]. Studies on model compounds indicate that changes to the local spin densities associated with structural rearrangements, such as changes to the ligand environment, could obscure a Mn-centered oxidative shift [29,44,45]. Minimal changes to the emission spectra, observed upon the $S_2 \rightarrow S_3$ transition in previous studies, were attributed to ligand-centered oxidation [35]. Low S_1 to S_2 state conversion following the first laser flash could produce equivalent changes in the S_1 to S_2 and S_2 to S_3 transitions observed by Zaharieva et al. [16], however, the origin of such discrepancies between reports has yet to be elucidated.

S_0 forms after O_2 evolution.

To probe samples enriched with S_0, XES spectra were collected after a 40 ms delay following a third laser flash, ($3F_{40ms}$). The first moment of $3F_{40ms}$ is consistently shifted to higher energies (Figure 3C, S3 & S4), supporting the expected reduction of Mn. Overall, the RT TR-XES results are in good agreement with previous Mn Kβ emission data [17,35]. Having validated the experimental technique, we investigated the elusive transient S_3 to S_0 process also initiated by three laser flashes (3F).

O-O bond formation step.

Figure 3 depicts the earliest evolution of the OEC electronic structure following three laser flashes and the associated first moment changes of Mn $K\beta_{1,3}$ measured at Δt ~50 μs ($3F_{50\mu s}$) and Δt ~200 μs ($3F_{200\mu s}$). The trend of increasing first moment is robust and statistically significant, Table 3 & Figures 3 & S4. It is important to note that this statistically significant change occurs after S_2 to S_3 transition, for which our analysis did *not* detect a statistically significant change in the spectra, Table 3 & Figure 2. Furthermore, the observed increase in the first moment cannot be explained by mixing of S-states due to poor protein advancement, as this would produce an oxidative (decrease in the first moment) trend or no change, see the SI for details regarding laser excitation. Based on the results of our statistical analysis, there is less than a 5% chance that this trend of increasing first moment is merely noise. It is extremely unlikely that we would repeatedly observe p-values less than 0.05 if we were prevented from detecting small spectral changes due to inherent limitations of our spectroscopic setup. Random reassignment of S-state labels, representative of datasets limited by spectrometer resolution, for example, yields p-values less than 0.05 in only 5% of the random assignments, which is the expected false positive rate. We are therefore confident

that these trends are not resolution limited. To further probe the robustness of the shifts, we repeated our analysis on randomly divided halves of the data and repeated our ANOVA analysis. Recovery of statistical significance after this procedure demonstrates that there is, in fact, a (5%)2 = 0.25% chance that the reported effect is due to noise.

This statistically significant spectral shift suggests that during the S_3 to S_0 transition the OEC undergoes a significant transformation at short timescales. Changes observed at 50 μs and 200 μs are likely due to a short-lived isoform of the S_3 state (S_3OO), in which the O-O bond has been formed and Mn centers have been reduced from the $(MnIV)_4$ state [46]. The accumulation of this species is controlled by its rate of formation (k_1), and rate of oxidation due to electron transfer to Tyr_Z• (k_2), which produces a one electron more oxidized S_4OO state, Figure 1E. The first moment of the Mn $K\beta_{1,3}$ line is commonly correlated with the nominal spin value of the Mn center, Figure 4. We observe that the nominal spin of $3F_{50\mu s}$ and $3F_{200\mu s}$ deviates from the all MnIV assignment reported for S_3 and represented on our plot by MnO_2 oxide as well as two model compounds containing a single MnIV center. Intriguingly, the shift between 2F and $3F_{200\mu s}$ is greater than that observed between 2F and $3F_{500\mu s}$, for which statistical significance was only visible on some plots (Figure 3) but was not strictly demonstrated in the 6.485–6.495 keV range. It is currently unclear whether this effect is rooted in statistical uncertainty, or is simply a weak spectral change due to transient oxidation of the OEC by electron transfer to Tyr_Z• (k_2) Figure 1E. Transient oxidation would likely temporarily pause or reverse the reductive (increasing) trend in first moments.

While density functional theory (DFT) modeling has proven inconclusive regarding the formation of a MnV=O species [22,24,47,48], we were unable to observe oxidation of the OEC, which would likely be associated with lower values of the first moment, at any observation time point following the third flash and measured over multiple beamtimes. This lack of evidence for oxidation past 2F (majority state S_3) was consistently observed (Figures 3, S3 & S4) thereby excluding formation of a $MnVMn_3IV$ state kinetic intermediate. Current DFT models [21–24] also do not resolve the previously identified kinetic challenge [20]. UV-Vis difference spectra show that Tyr_Z• is reduced quite slowly, ~1 ms after the third flash. Given that this time constant is comparable to the rate of O_2 evolution, only a very short ~50 μs time window remains for all bond formation dynamics and product/substrate exchange to occur.

Discussion

The TR-XES results detailed above cannot be explained by most DFT mechanistic models. Those which propose a Mn_4IV-O• (oxyl radical) in place of MnV=O, for example, predict significant activation barriers for O−O bond formation [21,25], in disagreement with spectroscopic results that show early onset reduction in both XES and XAS. Our results *are*, however, in agreement with the only other published TR studies probing the electronic structure evolution of the Mn centers via x-ray absorption spectroscopy (XAS) [13,16,49]. TR-XAS detected no oxidation and instead, suggests the gradual (milliseconds) reduction of the OEC initiated 250 μs into the S_3 to S_0 transition. In contrast to the XAS study, where only two energy points along the Mn K-edge were analyzed, we collected full spectra with high multiplicity, representing the complete electronic structure of the OEC at Δt ~50 μs and

Δt ~200 μs. In addition, XAS and XES probe different electronic transitions. It is therefore possible that some early spectral changes between t = 0–200 μs may have previously escaped detection, or are less pronounced in XAS due to the transient nature of the early intermediate. A more recent XES study performed at the Linac Coherent Light Source indicates no changes to the Mn Kβ spectra 250 μs after the third laser excitation [50]. We attribute this discrepancy to the differences in experimental conditions that will likely be clarified in the future.

To overcome the kinetic challenge, we proposed that the O−O formation step takes place in the S_3 to S_0 transition prior to the reduction of $TyrY_Z$•, Figure 1E [28,29]. Rapid evolution of the OEC during the S_3 to S_0 transition has long been a primary target of PS II research. Based on UV-Vis difference spectroscopy [15,51] and TR infrared spectroscopy [14] a deprotonation event has been proposed to occur early (0–300 μs) during this transition. Our results do not explicitly exclude a deprotonation event, but necessitate significant changes to the electronic structure of the 3*d* Mn frontier orbitals to explain the observed spectroscopic effect. The results presented here can be better rationalized if the formation of the $(TyrY_Z•)S_3$ state, occurring on the order of 100 ns [14], triggers a sequence of events resulting in significant redox or structural changes to the OEC, such as the formation of the O−O bond. The most recent isotope exchange studies show that substrate exchange stops early (0–300 μs) in the transition [19] hinting at such a possibility. The highest activation energies have also been noted in this early time window [52]. Likewise, the only molecularly defined system for water oxidation functioning with a comparative reaction rate, $[Ru(bda)(isoq)_2]$, is hypothesized to work via a radical coupling mechanism, which results in a peroxo intermediate. During the final catalytic step of this artificial system, the peroxo intermediate is further oxidized, and release of O_2 follows [53]. These results suggest that the same catalytic mechanism engenders rapid O_2 evolution in both biological and bio-mimetic systems, while at the same time preventing peroxide release due to the transient presence of the peroxo isoform.

In summary, to analyze the evolution of the photosystem II electronic structure, we observed intermediate states of photosynthetic O_2 production via microsecond resolution time-resolved x-ray emission spectroscopy at a synchrotron source. Consistent with the obtained full spectra is a mechanism involving the O−O bond formation in the S_3 to S_0 transition prior to $TyrY_Z$• reduction. This mechanism resolves the previously highlighted kinetic problems. Parallel advancements in the development of molecular catalysts for artificial photosynthesis strongly support O-O bond formation prior to the final oxidation step of such peroxo intermediates and provide further support for the mechanistic proposal detailed herein.

Supplementary Material

Refer to Web version on PubMed Central for supplementary material.

Acknowledgements

This research was supported by NSF, CHE-1350909 (Y.P.) and the NSF Graduate Research Fellowship under Grant No. DGE0833366 (K.D.). Research at the University of Washington is supported by the DOE, Office of Basic

Energy Sciences DE-SC0002194. PNC/XSD facilities at the Advanced Photon Source and research at these facilities are supported by the U.S. Department of Energy, Basic Energy Sciences, a Major Resources Support grant from NSERC, the University of Washington, Simon Fraser University, and the Advanced Photon Source. Use of the Advanced Photon Source, an Office of Science User Facility operated for the U.S. Department of Energy (DOE) Office of Science by Argonne National Laboratory, was supported by the U.S. DOE under Contract No. DE-AC02–06CH11357. Use of the BioCARS Sector 14 was also supported by grants from the National Center for Research Resources (5P41RR007707) and the National Institute of General Medical Sciences (8P41GM103543) from the National Institutes of Health. The time-resolved setup at BioCARS was funded in part through a collaboration with Philip Anfinrud (NIH/NIDDK). We thank Prof. L. Slipchenko from Purdue University for providing computational resources and helpful discussion.

References and Notes:

[1]. Kok B, Forbush B, and McGloin M, Cooperation of Charges in Photosynthetic Oxygen Evolution. I. A Linear Four Step Mechanism, Photochem. Photobiol 11, 457 (1970). [PubMed: 5456273]

[2]. Wydrzynski T and Satoh S, Photosystem II: The Light-Driven Water:Plastoquinone Oxidoreductase (Springer, Dordrecht, 2005), Advances in Photosynthesis and Respiration.

[3]. Ferreira KN, Iverson TM, Maghlaoui K, Barber J, and Iwata S, Architecture of the Photosynthetic Oxygen-Evolving Center, Science 303, 1831 (2004). [PubMed: 14764885]

[4]. Zouni A, Witt HT, Kern J, Fromme P, Krauss N, Saenger W, and Orth P, Crystal Structure of Photosystem II from Synechococcus elongatus at 3.8 Angstrom Resolution, Nature 409, 739 (2001). [PubMed: 11217865]

[5]. Guskov A, Kern J, Gabdulkhakov A, Broser M, Zouni A, and Saenger W, Cyanobacterial Photosystem II at 2.9-Angstrom Resolution and the Role of Quinones, Lipids, Channels and Chloride, Nat. Struct. Mol. Biol 16, 334 (2009). [PubMed: 19219048]

[6]. Pushkar Y, Yano J, Glatzel P, Messinger J, Lewis A, Sauer K, Bergmann U, and Yachandra V, Structure and Orientation of the Mn4Ca Cluster in Plant Photosystem II Membranes Studied by Polarized Range-Extended X-Ray Absorption Spectroscopy, J. Biol. Chem 282, 7198 (2007). [PubMed: 17190828]

[7]. Umena Y, Kawakami K, Shen JR, and Kamiya N, Crystal Structure of Oxygen-Evolving Photosystem II at a Resolution of 1.9 Angstrom, Nature 473, 55 (2011). [PubMed: 21499260]

[8]. Glockner C, Kern J, Broser M, Zouni A, Yachandra V, and Yano J, Structural Changes of the Oxygen-Evolving Complex in Photosystem II During the Catalytic Cycle, J. Biol. Chem 288, 22607 (2013). [PubMed: 23766513]

[9]. Kupitz C et al., Serial Time-Resolved Crystallography of Photosystem II Using a Femtosecond X-Ray Laser, Nature 513, 261 (2014). [PubMed: 25043005]

[10]. Suga M et al., Light-Induced Structural Changes and the Site of O=O Bond Formation in PSII Caught by XFEL, Nature 543, 131 (2017). [PubMed: 28219079]

[11]. Young ID et al., Structure of Photosystem II and Substrate Binding at Room Temperature, Nature 540, 453 (2016). [PubMed: 27871088]

[12]. Davis KM and Pushkar YN, Structure of the Oxygen Evolving Complex of Photosystem II at Room Temperature, J. Phys. Chem. B 119, 3492 (2015). [PubMed: 25621994]

[13]. Haumann M, Liebisch P, Muller C, Barra M, Grabolle M, and Dau H, Photosynthetic O2 Formation Tracked by Time-Resolved X-Ray Experiments, Science 310, 1019 (2005). [PubMed: 16284178]

[14]. Noguchi T, Suzuki H, Tsuno M, Sugiura M, and Kato C, Time-Resolved Infrared Detection of the Proton and Protein Dynamics During Photosynthetic Oxygen Evolution, Biochemistry 51, 3205 (2012). [PubMed: 22458839]

[15]. Rappaport F, Blancharddesce M, and Lavergne J, Kinetics of Electron-Transfer and Electrochromic Change During the Redox Transitions of the Photosynthetic Oxygen-Evolving Complex, Biochim. Biophys. Acta-Bioenerg 1184, 178 (1994).

[16]. Zaharieva I, Dau H, and Haumann M, Sequential and Coupled Proton and Electron Transfer Events in the S2 → S3 Transition of Photosynthetic Water Oxidation Revealed by Time-Resolved X-Ray Absorption Spectroscopy, Biochemistry 55, 6996 (2016). [PubMed: 27992997]

[17]. Zaharieva I, Chernev P, Berggren G, Anderlund M, Styring S, Dau H, and Haumann M, Room-Temperature Energy-Sampling Kβ X-Ray Emission Spectroscopy of the Mn4Ca Complex of Photosynthesis Reveals Three Manganese-Centered Oxidation Steps and Suggests a Coordination Change Prior to O2 Formation, Biochemistry 55, 4197 (2016). [PubMed: 27377097]

[18]. Babcock GT, Blankenship RE, and Sauer K, Reaction-Kinetics for Positive Charge Accumulation on Water Side of Chloroplast Photosystem, FEBS Lett. 61, 286 (1976). [PubMed: 174952]

[19]. Nilsson H, Rappaport F, Boussac A, and Messinger J, Substrate-Water Exchange in Photosystem II Is Arrested before Dioxygen Formation, Nature Comm. 5, 4305 (2014).

[20]. Kern J and Renger G, Photosystem II: Structure and Mechanism of the Water:Plastoquinone Oxidoreductase, Photosynth. Res 94, 183 (2007). [PubMed: 17634752]

[21]. Siegbahn PEM, Water Oxidation Mechanism in Photosystem II, Including Oxidations, Proton Release Pathways, O-O Bond Formation and O2 Release, Biochim. Biophys. Acta 1827, 1003 (2013). [PubMed: 23103385]

[22]. Saito T et al., Possible Mechanisms of Water Splitting Reaction Based on Proton and Electron Release Pathways Revealed for Camn4o5 Cluster of PSII Refined to 1.9 Angstrom X-Ray Resolution, Int. J. Quantum Chem 112, 253 (2012).

[23]. Yamaguchi K et al., Full Geometry Optimizations of the Mixed-Valence Camn4o4x(H2o)(4) (X=Oh or O) Cluster in Oec of PS II: Degree of Symmetry Breaking of the Labile Mn-X-Mn Bond Revealed by Several Hybrid Dft Calculations, Int. J. Quantum Chem 113, 525 (2013).

[24]. Sproviero EM, Gascon JA, McEvoy JP, Brudvig GW, and Batista VS, Quantum Mechanics/ Molecular Mechanics Study of the Catalytic Cycle of Water Splitting in Photosystem II, J. Am. Chem. Soc 130, 3428 (2008). [PubMed: 18290643]

[25]. Siegbahn PEM, O-O Bond Formation in the S4 State of the Oxygen-Evolving Complex in Photosystem II, Chem. Eur. J 12, 9217 (2006). [PubMed: 17029313]

[26]. Davis KM et al., Fast Detection Allowing Analysis of Metalloprotein Electronic Structure by X-Ray Emission Spectroscopy at Room Temperature, J. Phys. Chem. Lett 3, 1858 (2012). [PubMed: 22919444]

[27]. Kern J et al., Simultaneous Femtosecond X-Ray Spectroscopy and Diffraction of Photosystem II at Room Temperature, Science 340, 491 (2013). [PubMed: 23413188]

[28]. Davis KM et al., Rapid Evolution of the Photosystem II Electronic Structure During Water Splitting, arXiv:1506.08862 (2015).

[29]. Jensen SC et al., X-Ray Emission Spectroscopy of Biomimetic Mn Coordination Complexes, J. Phys. Chem. Lett 8, 2584 (2017). [PubMed: 28524662]

[30]. Bai X.-c., McMullan G, and Scheres SHW, How Cryo-Em Is Revolutionizing Structural Biology, Trends Biochem. Sci 40, 49. [PubMed: 25544475]

[31]. Glatzel P and Bergmann U, High Resolution 1s Core Hole X-Ray Spectroscopy in 3d Transition Metal Complexes - Electronic and Structural Information, Coord. Chem. Rev 249, 65 (2005).

[32]. Davis KM, Kosheleva I, Henning RW, Seidler GT, and Pushkar Y, Kinetic Modeling of the X-Ray-Induced Damage to a Metalloprotein, J. Phys. Chem. B 117, 9161 (2013). [PubMed: 23815809]

[33]. Mattern BA, Seidler GT, Haave M, Pacold JI, Gordon RA, Planillo J, Quintana J, and Rusthoven B, A Plastic Miniature X-Ray Emission Spectrometer (miniXES) Based on the Cylindrical Von Hamos Geometry, Rev. Sci. Instrum 83, 023901 (2012). [PubMed: 22380101]

[34]. Messinger J, Schroder WP, and Renger G, Structure-Function Relations in Photosystem-II - Effects of Temperature and Chaotropic Agents on the Period 4 Oscillation of Flash-Induced Oxygen Evolution, Biochemistry 32, 7658 (1993). [PubMed: 8347576]

[35]. Messinger J et al., Absence of Mn-Centered Oxidation in the S_2 to S_3 Transition:Implications for the Mechanism of Photosynthetic Water Oxidation, J. Am. Chem. Soc 123, 7804 (2001). [PubMed: 11493054]

[36]. Pushkar Y, Yano J, Sauer K, Boussac A, and Yachandra VK, Structural Changes in the Mn4Ca Cluster and the Mechanism of Photosynthetic Water Splitting, P. Natl. Acad. Sci 105, 1879 (2008).

[37]. Alonso-Mori R et al., Towards Characterization of Photo-Excited Electron Transfer and Catalysis in Natural and Artificial Systems Using Xfels, Faraday Discuss. 194, 621 (2016). [PubMed: 27711803]

[38]. Fuller FD et al., Drop-on-Demand Sample Delivery for Studying Biocatalysts in Action at X-Ray Free-Electron Lasers, Nat. Meth 14, 443 (2017).

[39]. Ono T.-a., Noguchi T, Inoue Y, Kusunoki M, Matsushita T, and Oyanagi H, X-Ray Detection of the Period-Four Cycling of the Manganese Cluster in Photosynthetic Water Oxidizing Enzyme, Science 258, 1335 (1992). [PubMed: 17778358]

[40]. Iuzzolino L, Dittmer J, Dörner W, Meyer-Klaucke W, and Dau H, X-Ray Absorption Spectroscopy on Layered Photosystem II Membrane Particles Suggests Manganese-Centered Oxidation of the Oxygen-Evolving Complex for the S_0-S_1, S_1-S_2, and S_2-S_3 Transitions of the Water Oxidation Cycle, Biochemistry 37, 17112 (1998). [PubMed: 9860823]

[41]. Haumann M, Muller C, Liebisch P, Iuzzolino L, Dittmer J, Grabolle M, Neisius T, Meyer-Klaucke W, and Dau H, Structural and Oxidation State Changes of the Photosystem II Manganese Complex in Four Transitions of the Water Oxidation Cycle (S-0 → S-1, S-1 → S-2, S-2 → S-3, and S-3,S-4 → S-0) Characterized by X-Ray Absorption Spectroscopy at 20 K and Room Temperature, Biochemistry 44, 1894 (2005). [PubMed: 15697215]

[42]. Cox N, Retegan M, Neese F, Pantazis DA, Boussac A, and Lubitz W, Electronic Structure of the Oxygen Evolving Complex in Photosystem II Prior to O-O Bond Formation, Science 345, 804 (2014). [PubMed: 25124437]

[43]. Schuth N, Zaharieva I, Chernev P, Berggren G, Anderlund M, Styring S, Dau H, and Haumann M, Kα X-Ray Emission Spectroscopy on the Photosynthetic Oxygen-Evolving Complex Supports Manganese Oxidation and Water Binding in the S3 State, Inorg. Chem (2018).

[44]. Davis KM, Palenik MC, Yan L, Smith PF, Seidler GT, Dismukes GC, and Pushkar YN, X-Ray Emission Spectroscopy of Mn Coordination Complexes Towards Interpreting the Electronic Structure of the Oxygen Evolving Complex of Photosystem II, J. Phys. Chem. C 120, 3326 (2016).

[45]. Vanko G, Neisius T, Molnar G, Renz F, Karpati S, Shukla A, and de Groot FMF, Probing the 3d Spin Momentum with X-Ray Emission Spectroscopy: The Case of Molecular-Spin Transitions, J. Phys. Chem. B 110, 11647 (2006). [PubMed: 16800459]

[46]. Pushkar Y, Davis KM, and Palenik MC, Model of the Oxygen Evolving Complex Which Is Highly Predisposed to O–O Bond Formation, J. Phys. Chem. Lett 9, 3525 (2018). [PubMed: 29863871]

[47]. Yamanaka S et al., Structure and Reactivity of the Mixed-Valence CaMn4O5(H2O)(4) and CaMn4O4(OH)(H2O)(4) Clusters at Oxygen Evolution Complex of Photosystem II. Hybrid Dft (UB3LYP and UBHandHLYP) Calculations, Int. J. Quantum Chem 112, 321 (2012).

[48]. Yamanaka S et al., Possible Mechanisms for the O-O Bond Formation in Oxygen Evolution Reaction at the CaMn4O5(H2O)(4) Cluster of PSII Refined to 1.9 Angstrom X-Ray Resolution, Chem. Phys. Lett 511, 138 (2011).

[49]. Haumann M, Grundmeier A, Zaharieva I, and Dau H, Photosynthetic Water Oxidation at Elevated Dioxygen Partial Pressure Monitored by Time-Resolved X-Ray Absorption Measurements, P. Natl. Acad. Sci 105, 17384 (2008).

[50]. Kern J et al., Taking Snapshots of Photosynthetic Water Oxidation Using Femtosecond X-Ray Diffraction and Spectroscopy, Nat. Comm 5, 4371 (2014).

[51]. Haumann M, Bogershausen O, Cherepanov D, Ahlbrink R, and Junge W, Photosynthetic Oxygen Evolution: H/D Isotope Effects and the Coupling between Electron and Proton Transfer During the Redox Reactions at the Oxidizing Side of Photosystem II, Photosynth. Res 51, 193 (1997).

[52]. Bao H and Burnap RL, Structural Rearrangements Preceding Dioxygen Formation by the Water Oxidation Complex of Photosystem II, P. Natl. Acad. Sci 112, E6139 (2015).

[53]. Duan L, Bozoglian F, Mandal S, Stewart B, Privalov T, Llobet A, and Sun L, A Molecular Ruthenium Catalyst with Water-Oxidation Activity Comparable to That of Photosystem II, Nat. Chem 4, 418 (2012). [PubMed: 22522263]

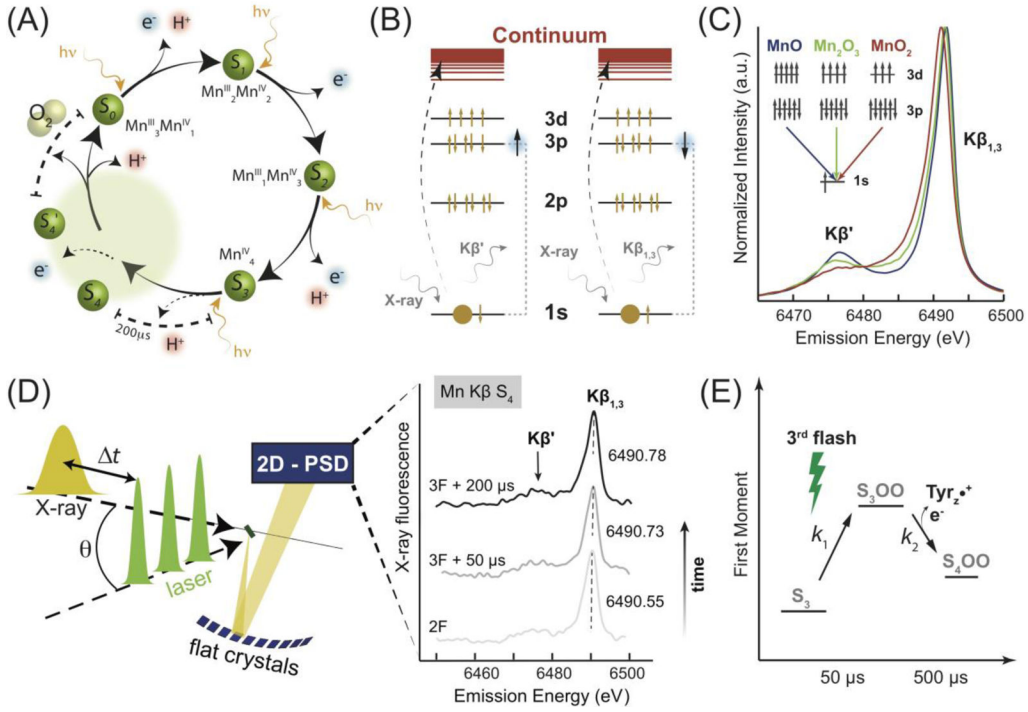

Figure 1. Schematic outline of the TR-XES experimental setup.

(A) Current model of the Kok cycle. Depiction of sequential incident visible light photon absorptions triggering electron/proton release [13]. The dashed region is based on previous analysis of the S_3 to S_0 transition in which the S_4 state was proposed [13,49]. **(B)** Electronic transitions, reflected in the Kβ main lines, are influenced by the spin state of the Mn ion. **(C)** A spectral comparison of Mn oxides depicts the effect of changing oxidation state on the Kβ emission lines**. (D)** Nanosecond laser pulses (1, 2 or 3) are used to advance the Kok cycle in the protein, Table S1. The pump/probe delay time, Δ*t*, measured from the final laser flash to the center of the x-ray pulse, is set dependent on the desired S-state. X-ray fluorescence from the sample is reflected by 10 flat analyzer crystals onto a 2D-position sensitive detector. Kβ emission spectra are extracted to form snapshots of the electronic structure in time. Smoothed emission spectra are presented for 2F (majority S_3) and two time points during the S_3 to S_0 transition. (**E**) The proposed reaction scheme shows the early evolution of the OEC during the S_3 to S_0 transition, providing an interpretation of spectroscopic results.

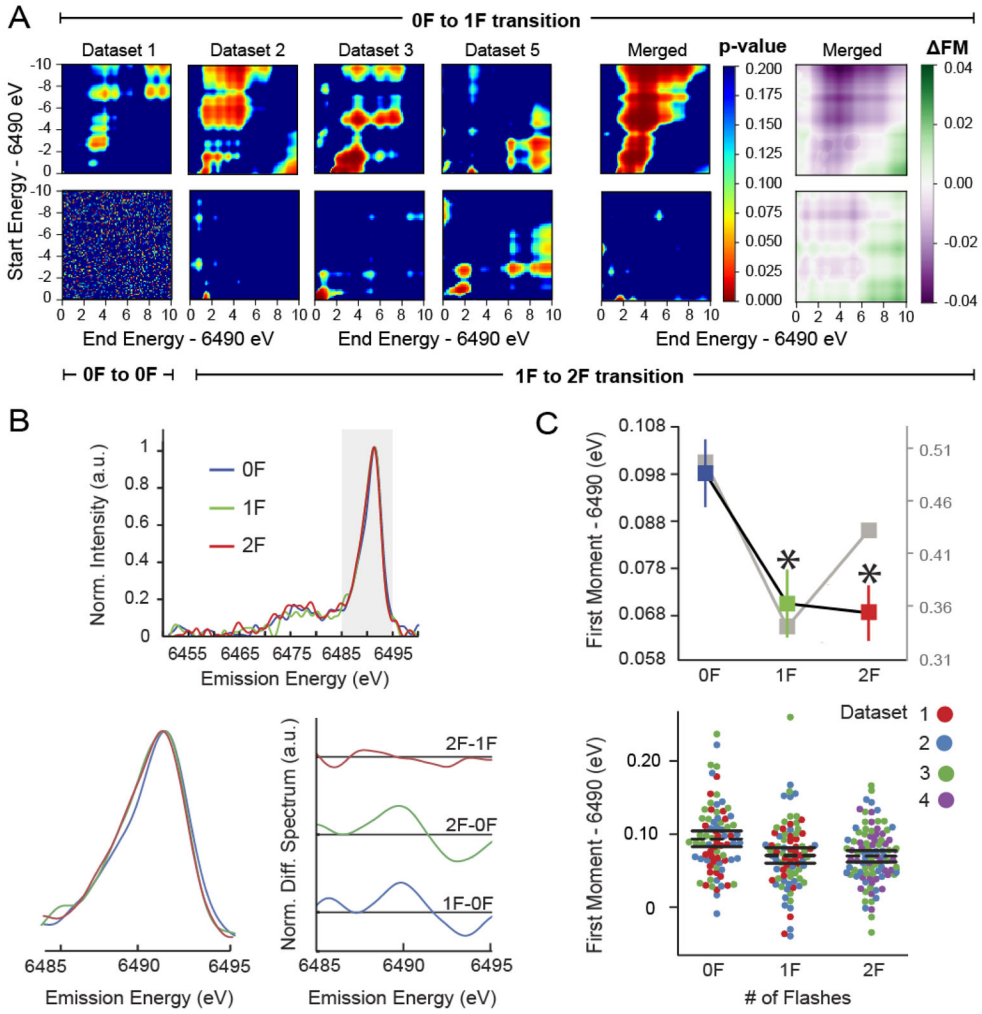

Figure 2. Analysis of statistical significance for $S_1 \rightarrow S_2 \rightarrow S_3$ transitions serves as a proof of concept.

(A) Spectral shifts occurring as a result of 0F→1F and 1F→2F transitions are characterized using 2-D heatmaps, illustrating the p-value (see Table S2 for *n*) for changes to first moments calculated over the ranges defined by the x and y axes, i.e. start and end energy, respectively. Contours appear in plots comparing 0F→1F data indicate statistically significant difference. By contrast, limited low p-value regions are observed for the 1F→2F transition, suggesting a smaller change. The directionality and magnitude of spectral shifts are shown in the final column. These 2-D heatmaps, which graphically illustrate the change in first moments ($\Delta FM = FM_{post\text{-}flash} - FM_{pre\text{-}flash}$) calculated over the ranges defined by the x and y axes. 0F→1F and 1F→2F transitions are dominated by positive, or oxidative, shifts. An example of statistical noise is presented by randomly dividing a 0F dataset and performing the same analysis, e.g. 0F→0F. Relevant data from datasets 1–4 were merged to generate the final columns. Note that 0F and 1F data were not collected for dataset 4, while dataset 5 was collected independently following beamline upgrade and is therefore analyzed separately, see Fig. S4. **(B)** Wavelet-transform smoothed via wavelet transforms and background subtracted emission spectra for merged 0–2F data. The region (6.485–6.495

keV) over which the first moment was calculated is highlighted and a magnified inset as well as difference spectra are presented. Difference spectra were smoothed with a rolling average calculated over 14 points (~ ±0.7 eV). (**C**) (*left*) Average first moments from unprocessed (color) and processed (grey) spectra. Errors are presented as SEM with n given in Table 2. Those moments with a statistically significant difference ($p<0.05$) from 0F data are indicated with an asterisk. (*right*) Dot plot of first moments from raw data. Each dot represents a calculated first moment from a thread collected during the beamtime corresponding to its color in the legend. Dashed lines represent the average first moment while solid bars are the 95% confidence interval.

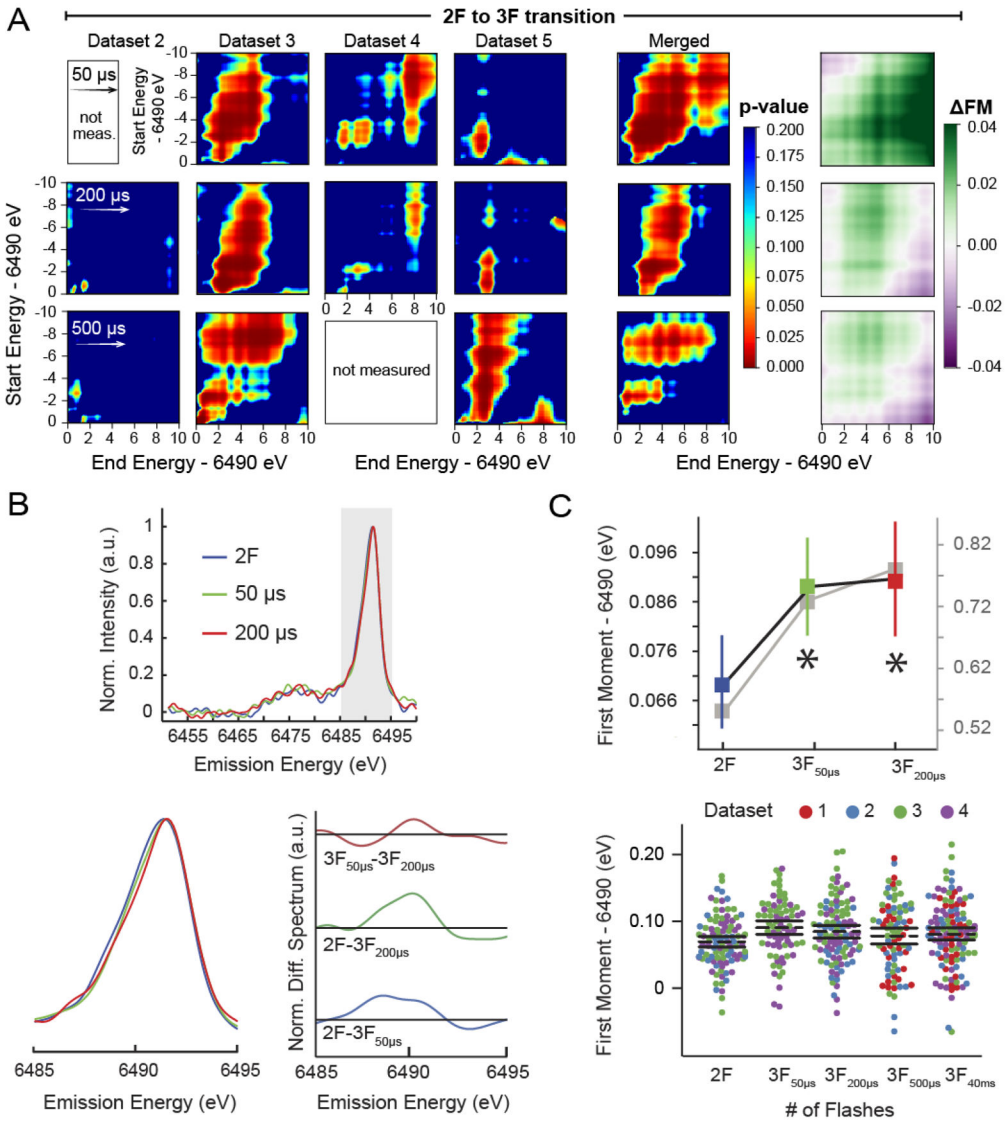

Figure 3. Rapid onset of spectral changes observed during the S_3 to S_0 transition.

(A) Spectral shifts occurring as a result of the 2F→3F transition are characterized using 2-D heatmaps colored by p-value (see Table S2 for *n*), for changes to first moments calculated over the ranges defined by the x and y axes, i.e. start and end energy, respectively. Strong contours are consistently observed indicative of a statistically significant spectral change. The directionality and magnitude of spectral shifts occurring with these transitions are also shown as 2-D heatmaps, which graphically illustrate the change in first moments ($\Delta FM=FM_{post\text{-}flash}-FM_{pre\text{-}flash}$) calculated over the ranges defined by the x and y axes. All 2F→3F comparisons yield primarily negative, or reductive, shifts. Determined p-values ~0.02 (Table 3) for the 200 µs time point are further supported by the above heatmaps, however, little information can be gleaned from these plots of dataset 2, likely due to much lower x-ray shot count, see Table 2. Although the 500 µs time point is equally compelling, the traditional energy range (6.485–6.495 keV) selected for reporting first moments does not deliver statistical significance, Table 3. **(B)** Wavelet transform smoothed and background

subtracted emission spectra for merged 2–3F data, calculated as in Fig. 2B. (**C**) (*left*) Average first moments from unprocessed (color) and processed (grey) spectra. Errors are presented as SEM with n given in Table 2. Those moments with a statistically significant difference ($p<0.05$) from 2F data are indicated with an asterisk. (*right*) Dot plot of first moments from raw data, presented as in Fig. 2C. See Fig. S3 for 2-D plots of the 40 ms (majority S_0 state) time point.

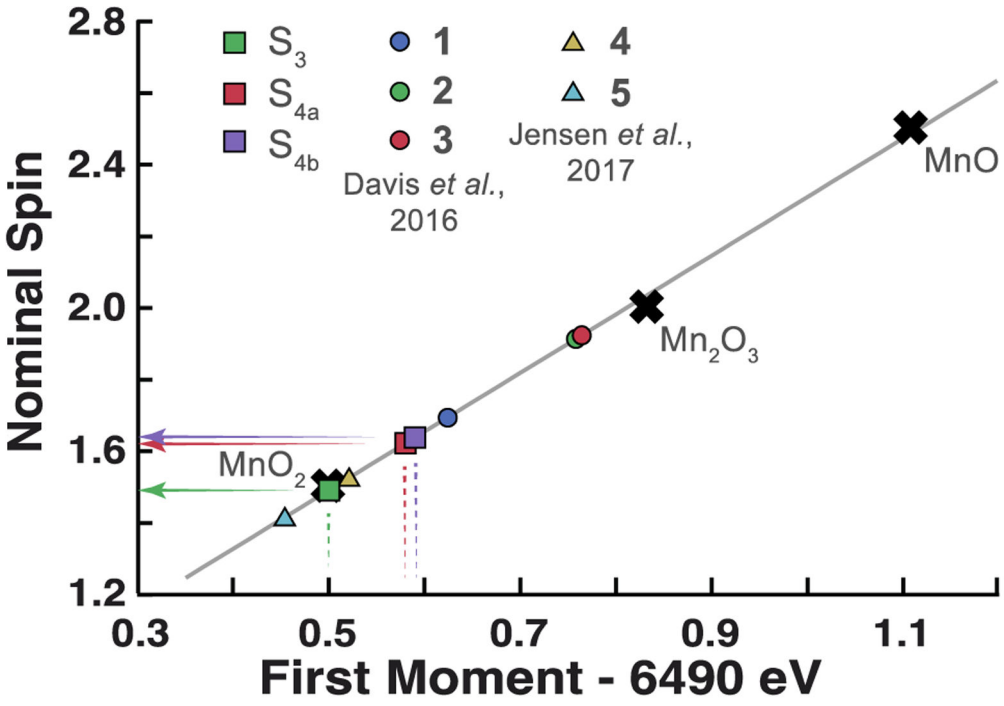

Figure 4. Analysis of Mn Kβ first moments.

Placement of fully processed 2F/3F data along a linear fit to a series of Mn oxide first moments empirically predicts the average spin state of Mn centers in the OEC. For reference, relevant Mn coordination complexes are placed along the line by using the nominal spins reported by Davis *et al.* and Jensen *et al.* [29,44]. Note that S_{4a} and S_{4b} correspond to 3F states with Δt between the final laser flash and x-ray pulse of 50 μs and 200 μs, respectively. Compounds **1**–**3** are formally mixed valence MnIII/MnIV complexes. **1** is a di-μ-oxo dimer, $[Mn_2O_2L'_4](ClO_4)_3$, while **2** and **3** are two examples from the Mn cubane family, $Mn_4O_4L_6$. Compounds **4** and **5**, by contrast, are mononuclear Mn complexes $[MnIV(OH)_2(Me_2EBC)]2+$ and $[MnIV(O)(OH)\text{-}(Me_2EBC)]+$, respectively.

Table 1.

Experimental characteristics of pulsed x-ray source

Characteristics	BioCARS
Excitation Energy	Peak energy 7.85 keV, FWHM ~500 eV
X-ray Spot Size	~45 × 100 μm2
Pulse Length	44 μs (22 μs dataset 5)
Photon Flux	3 × 1011 photons/pulse
Dose Delivered per Pulse	~7 × 107 photons/μm2

Table 2.

Approximate number of x-ray pulses per state, per beamtime.

Majority S-State	Flash	Data Sets					
		1	2	3		4	5**
S_0	$3F_{40ms}$	43,250	60,000	55,333		107,222	97,800
S_1	0	62,267	72,800	60,233		n/a	100,000
S_2	1	42,083	61,556	55,333		n/a	88,900
S_3	2	n/a	62,000	57,178	48,889	107,222	95,600
S_{4a}	$3F_{50\mu s}$	n/a	n/a	57,178	48,889	111,667	93,300
S_{4b}	$3F_{200\mu s}$	n/a	60,889	57,178	48,889	110,556	86,700
S'_4	$3F_{500\mu s}$	43,750	60,889	57,400		n/a	91,100
Total		191,350	322,334	546,500		436,667	653,400

*Additional statistics were collected for S_3, S_{4a} and S_{4b} for data set 3. The columns are split to reflect the additional x-ray pulses for these states.

**This dataset was collected after 2015 upgrades to the optics at the BioCARS beamline which made impossible the use of the old experimental conditions and required twice shorter (1/2 intensity) pulses to minimize heat load on new optics components.

Table 3.

p- and F-values from ANOVA for state-to-state comparisons from data sets 1–4 combined.

Majority S-State (n)		**S_0**	**S_1**	**S_2**	**S_3**	**S_{4a}**	**S_{4b}**	**S'_4**
	Flash	**$3F_{40ms}$**	**0F**	**1F**	**2F**	**$3F_{50\mu s}$**	**$3F_{200\mu s}$**	**$3F_{500\mu s}$**
S_0 (117)	**$3F_{40ms}$**	1	0.08 (3.06)	0.06 (2.19)	0.06 (3.60)	0.17 (1.82)	0.63 (0.23)	0.66 (0.19)
S_1 (78)	**0F**		1	<0.01 (9.00)	<0.01 (13.56)	0.68 (0.17)	0.19 (1.67)	0.05 (3.80)
S_2 (81)	**1F**			1	0.85 (0.04)	<0.01 (7.27)	0.02 (3.68)	0.98 (0.82)
S_3 (96)	**2F**				1	<0.01 (11.32)	0.02 (5.87)	0.22 (1.50)
S_{4a} (75)	**$3F_{50\mu s}$**					1	0.11 (0.80)	0.18 (2.60)
S_{4b} (98)	**$3F_{200\mu s}$**						1	0.39 (0.73)
S'_4 (82)	**$3F_{500\mu s}$**							1

*p-values are based on the first moments over the range 6.485 – 6.495 keV. The number of “samples” (i.e. threads) is shown in parentheses for each state. These values are broken down by beamtime in Table S2. See Table 2 for additional comparisons between the states based on the number of x-ray pulses per state per beamtime and Figures 2C & 3C for dotplots of all first moments used for p-value calculations. F values are given in parentheses and, as each value represents comparison between only two groups, can be taken as $F(1,n_1+n_2-2)=F$ with n_e, n_2 being the number of measurements in the table. Analysis of data set 5 is shown in Fig. S4.